Journal of The Electrochemical Society, **149** (3) G184-G188 (2002)
0013-4651/2002/149(3)/G184/5/$7.00 © The Electrochemical Society, Inc.

Implantation Induced Defects in the Retrograde Well with a Buried Layer

Wei-Cheng Hsu,[a,z] Mong-Song Liang,[b] and Mao-Chieh Chen[a,*]

[a]*Department of Electronics Engineering, National Chiao Tung University, Hsinchu 300, Taiwan*
[b]*Taiwan Semiconductor Manufacturing Company, Research and Development Department, Advanced Module Technology Division, Hsinchu, Taiwan*

This work investigates the implantation induced extended defects in the retrograde p- and n-well with/without a buried layer after postimplantation thermal annealing at 950°C in N_2 ambient. A preferential etchant of CrO_3/HF mixed solution was used to delineate the defects induced by high-energy ion implantation. It is found that the extended defects elongated to the top surface of the retrograde well with a buried layer, which was implanted with high-energy boron ion at 1500 keV to a dose of 3×10^{13} cm^{-2}, resulting in the etching pits of extended defects at a density of about 10^5 cm^{-2}.
 [DOI: 10.1149/1.1445433]

Manuscript submitted May 14, 2001; revised manuscript received September 7, 2001. Available electronically January 30, 2002.

A retrograde well has been extensively utilized in the very large scale integrated (VLSI) circuits because of its advantages of chip size reduction, low thermal budget, process simplification, and improvements of surface topography and device performance.[1-10] Many device characteristics, such as hot carrier generation, channel mobility, punchthrough voltage, junction capacitance, latchup susceptibility, and soft error immunity can be improved and/or optimized by multiple-chain high-energy ion implantations.[8-10] In the deep submicrometer regime, a retrograde well with a buried layer formed by a megaelectronvolt ion implantation that replaces the use of an epi layer has been used to obtain a latchup-free condition.[11-15]

However, extended defects (including both dislocation and dislocation loops) were introduced by the multiple-chain high-energy ion implantation used to implement the retrograde well with a buried layer. The main issue of concern about the high-energy ion implantation in Si is the extended defects in the substrates that were formed in the postimplantation thermal annealing process.[16-20] The technique most utilized to investigate the defects induced by ion implantation is cross-sectional transmission electron microscopy (XTEM). However, the fabrication procedure of the TEM samples is complicated and time consuming. Moreover, XTEM cannot detect the defects at a density below 10^7 cm^{-2}, so that the presence of a low density of defects will probably be overlooked in the XTEM observation, yet such a low density of defects in the device junction region may be detrimental to its performance.[20] In our previous work, we developed a simple and effective method to delineate the residual defects in the high-energy ion implanted substrate after the postimplantation thermal annealing process.[21]

In this work, we use this previously developed method to detect and look into the extended defects generated by the processing of the retrograde well with a buried layer. A preferential chemical etching solution consisting of CrO_3 and HF acid was used for the defect delineation. Extended defects near the substrate's surface were found in the samples of a retrograde well with a buried layer after the samples were thermally annealed at temperatures lower than 1000°C.

Experimental

The substrates used for the experiments of this work were (100) oriented, p-type silicon wafers of 8 in. diam with 2-5 Ω-cm nominal resistivity. After the initial standard wafer cleaning, one group of wafers were implanted with boron ions at 1500 keV to a dose of 3×10^{13} cm^{-2} to simulate the buried layer implantation. This was followed by a series of four boron ion implantations performed in sequence at an energy/dose of 800 keV/3×10^{13} cm^{-2}, 180 keV/1×10^{13} cm^{-2}, 100 keV/7×10^{12} cm^{-2}, and 15 keV/6×10^{12} cm^{-2} to complete the simulation of implantation for the construction of a retrograde p-well with a buried layer. The other group of wafers underwent only three lower energy boron ion implantations of 180 keV/1×10^{13} cm^{-2}, 100 keV/7×10^{12} cm^{-2}, and 15 keV/6×10^{12} cm^{-2} in sequence to simulate the construction of a retrograde p-well without the buried layer. For the construction of a retrograde n-well, one group of wafers was also implanted with boron ions at an energy/dose of 1500 keV/3×10^{13} cm^{-2} to simulate the buried layer implantation. This was followed by a series of three phosphorus ion implantations performed in sequence at energy/dose of 800 keV/3×10^{13} cm^{-2}, 220 keV/5×10^{12} cm^{-2}, and 100 keV/1.5×10^{12} cm^{-2}, and an arsenic ion implantation performed at an energy/dose of 50 keV/1.5×10^{12} cm^{-2} to complete the simulation of implantation for the construction of a retrograde n-well with a buried layer. The other group of wafers underwent only three lower energy phosphorus ion implantations of 500 keV/1×10^{13} cm^{-2}, 220 keV/5×10^{12} cm^{-2}, and 100 keV/1.5×10^{12} cm^{-2}, and an arsenic ion implantation of 50 keV/1.5×10^{12} cm^{-2} in sequence to simulate the construction of a retrograde n-well without the buried layer. Table I summarizes the implantation conditions for the samples with a retrograde p-well (designated as sample 1), a retrograde p-well with a buried layer (designated as sample 2), a retrograde n-well (designated as sample 3), and a retrograde n-well with a buried layer (designated as sample 4), while Fig. 1 shows the schematic diagrams of these samples. All samples were thermally annealed in a furnace at 950°C for 30 min in an N_2 ambient. After the thermal annealing, each wafer was cut into pieces 1×1 cm square for defect delineation with preferential chemical etching. Prior to the chemical etching, the samples were dipped in flowing deionized (DI) water for 5 min to remove particles that may adhere to the surfaces of the samples and hence disturb the etching process. The samples were etched in a preferential etching solution consisting of one volume part of 0.15 M CrO_3 in DI water and two volume parts of HF (49%). The etching time ranged from 10 s to 1 min. During the etching process, the samples were properly agitated in the etching solution to prevent gas bubbles from gathering on the sample surfaces, which could disturb the etching results. After the etching, the samples were dipped in flowing DI water for 5 min. A scanning electron microscopy (SEM) was used to observe the surface morphology as well as the cross-sectional microstructure, and secondary ion mass spectrometer (SIMS) was used for elemental depth profile measurement. The program of transport of ions in matter (TRIM 92) was used to simulate the depth profiles of displaced Si induced by ion implantation.

* Electrochemical Society Active Member.
z E-mail: wchsu.ee85g@nctu.edu.tw

Table I. Ion implantations for retrograde well with/without buried layer.

	Ion/Energy/Dose
Retrograde p-well, sample 1	B/180 keV/1 × 10^{13} cm^{-2}
	B/100 keV/7 × 10^{12} cm^{-2}
	B/15 keV/6 × 10^{12} cm^{-2}
Retrograde p-well with buried layer, sample 2	B/1500 keV/3 × 10^{13} cm^{-2}
	B/800 keV/3 × 10^{13} cm^{-2}
	B/180 keV/1 × 10^{13} cm^{-2}
	B/100 keV/7 × 10^{12} cm^{-2}
	B/15 keV/6 × 10^{12} cm^{-2}
Retrograde n-well, sample 3	P/500 keV/1 × 10^{13} cm^{-2}
	P/220 keV/5 × 10^{12} cm^{-2}
	P/100 keV/1.5 × 10^{12} cm^{-2}
	As/50 keV/1.5 × 10^{12} cm^{-2}
Retrograde n-well with buried layer, sample 4	B/1500 keV/3 × 10^{13} cm^{-2}
	P/800 keV/3 × 10^{13} cm^{-2}
	P/220 keV/5 × 10^{12} cm^{-2}
	P/100 keV/1.5 × 10^{12} cm^{-2}
	As/50 keV/1.5 × 10^{12} cm^{-2}

Results and Discussion

Retrograde p-well with/without buried layer.—Figure 2 shows the top view and cross-sectional view SEM micrographs for sample 1 etched in the preferential etchant for 30 s, corresponding to the removal of a 0.3 μm thick surface layer from the Si wafer. The top view shows a rough surface at 40,000 times magnification and the cross-sectional view reveals an etching band of about 0.3 μm width extending from the etched Si surface. The corresponding SEM micrographs for the high energy ion implanted sample 2 etched in the preferential etchant for 30 s, are illustrated in Fig. 3. Etching pits can be seen clearly on the surface of sample 2; this is different from the surface of sample 1, where no etching pit is found (Fig. 2a). With prolonged etching using the preferential etchant, it is found that the density of the etching pits is about 5 × 10^5 cm^{-2}. From the cross-sectional view SEM micrograph of sample 2, it can be seen that, in addition to the etching band extending from the Si surface, there are two more obvious bands of striation, the distances from the top of which to the etched substrate surface are measured to be 0.7 and 1.4 μm (Fig. 3c). It is apparent that the top etching band arose from the series of low energy boron ion implantations at 180, 100, and 15 keV, while the bands at 0.7 and 1.4 μm from the top surface are obviously due to the 800 and 1500 keV high energy boron ion implantations, respectively.

Figure 4 shows the SIMS depth profile of the boron concentration for sample 2 after thermal annealing at 950°C for 30 min in N_2 ambient and the depth profile of displaced Si atoms introduced by each individual ion implantation obtained from the TRIM simulation. The etching bands of striation resulting from the 30 s etching are indicated by the hatched area. It is found that the locations of the

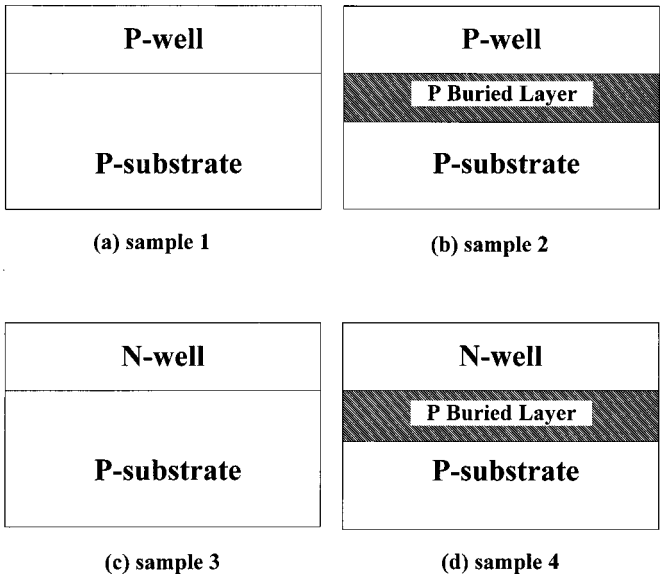

Figure 1. Schematic cross section of (a) sample 1, (b) sample 2, (c) sample 3, and (d) sample 4.

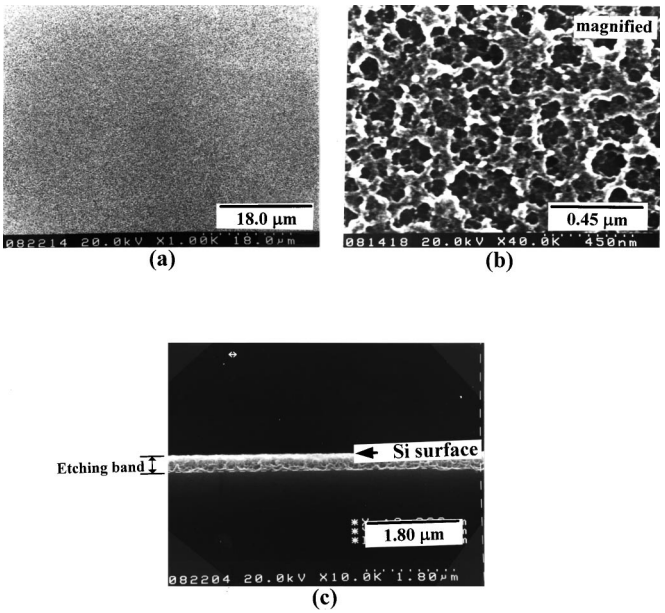

Figure 2. SEM micrographs showing (a) top view, (b) top view (magnified), and (c) cross-sectional view of sample 1 etched in preferential etchant for 30 s.

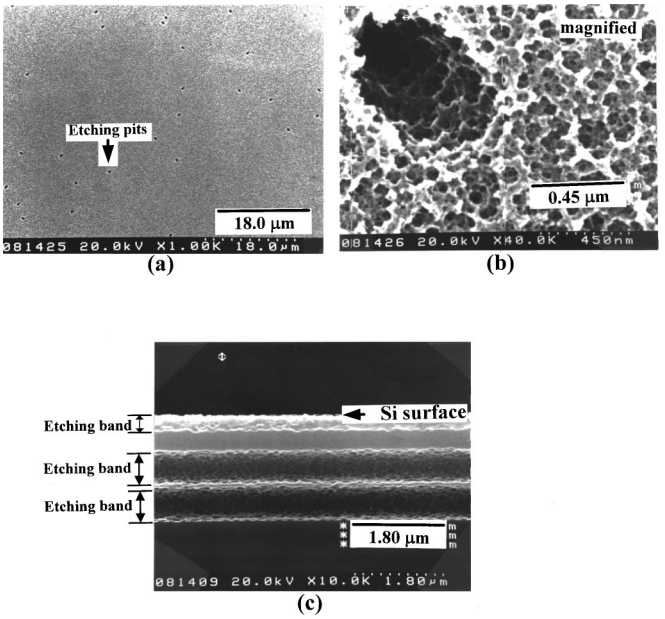

Figure 3. SEM micrographs showing (a) top view, (b) top view (magnified), and (c) cross-sectional view of sample 2 etched in preferential etchant for 30 s.

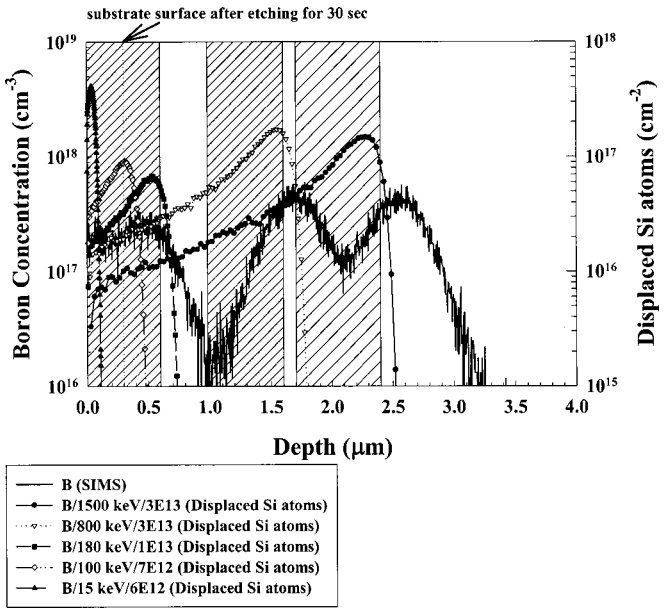

Figure 4. SIMS depth profile of boron concentration after thermal annealing at 950°C for 30 min in N_2 ambient and depth profile of displaced Si atoms obtained from TRIM simulation for sample 2.

bands of striation coincide with the depth profile of displaced Si atoms obtained from the TRIM simulation, indicating the direct relation between the secondary defect and the implantation damage. The striation bands at 1.7 to 2.4 μm, 1 to 1.6 μm, and 0 to 0.6 μm depth from the original Si substrate surface apparently resulted, respectively, from the 1500, and 800 keV, and the three lower energy, 180, 100, and 15 keV, boron ion implantations.

The criterion for extended defect formation by ion implantation is that the displaced Si atoms generated by the ion implantation exceed a critical number. It has been reported that the critical number of displaced Si atoms induced by boron ion implantation that would result in extended defect formation is about 1.5×10^{16} cm^{-2}.[22] For the case of sample 1, the displaced Si atoms generated by each ion implantation all exceed the critical number. Thus, the three successive boron ion implantations generated a sufficiently large number of interstitial Si atoms, that evolved to the extended defects during the thermal anneal, resulting in a rough surface and an etching band of striations, as revealed by the preferential etching shown in Fig. 2.

For sample 2, which is a p-retrograde well with a buried layer, there are etching pits on the surface. It was reported that the high energy boron ion implantation, with the implantation dose in excess of the threshold dose of 2×10^{13} cm^{-2}, will induce dislocations at the end of the projected range, and the dislocation will elongate along the ⟨110⟩ direction to the top surface region of the wafer;[20] moreover, it will also induce buried defects which are composed of dislocation loops beneath the substrate surface.[17] As a result, etching pits near the substrate surface and etching bands of striation can be seen, respectively, on the surface and in the cross section of sample 2 after the preferential etching. The etching pit is attributed to the dislocation which resulted from the two high-energy (1500 and 800 keV) boron ion implantations and subsequently elongated to the top surface of the Si substrate. Moreover, the three lower energy (180, 100, and 15 keV) boron ion implantations, and the 800 and 1500 keV high-energy implantations resulted in, respectively, the top, center, and bottom etching bands of striation after the preferential etching (Fig. 3c).

Retrograde n-well with/without buried layer.—Figure 5 shows the top view and cross-sectional view SEM micrographs for sample 3 etched in the preferential etchant for 30 s, corresponding to the

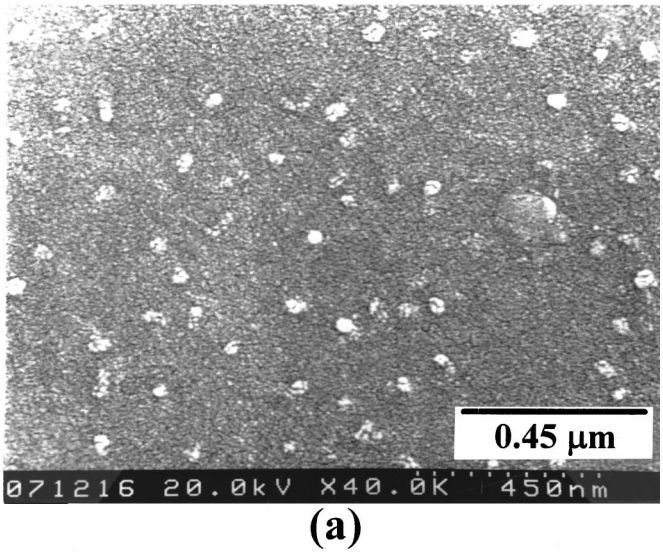

(a)

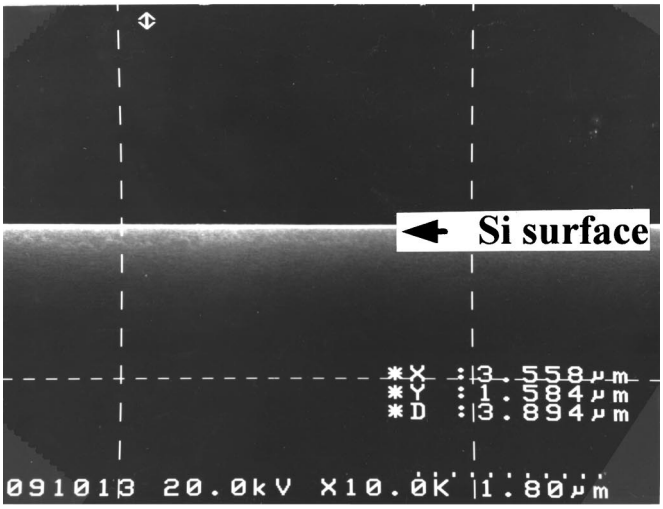

(b)

Figure 5. SEM micrographs showing (a) top view and (b) cross-sectional view of sample 3 etched in preferential etchant for 30 s.

removal of a 0.3 μm thick surface layer from the Si wafer. The sample shows a very smooth surface except for the appearance of white mounded artifacts and no obvious etching band in the cross-sectional view. Figure 6 shows the top view and cross-sectional view SEM micrographs for sample 4 etched in the preferential etchant for 30 s. Etching pits can be seen clearly on the surface of sample 4, whereas no etching pit is found on the surface of sample 3. With prolonged etching using the preferential etchant, it is found that the density of the etching pits is about 3×10^5 cm^{-2}. From the cross-sectional view SEM micrograph of sample 4, we found two bands of striations, one extending from the etched substrate surface and the other is located 1.6 μm below the surface.

Figure 7 shows the SIMS depth profiles of B, P, and As concentrations for sample 4 after thermal annealing at 950°C for 30 min in N_2 ambient and the depth profile of displaced Si atoms introduced by each individual ion implantation obtained from the TRIM simulation. The etching bands of striation resulting from the 30 s etching are indicated by the hatched area. It is obvious that the striation band at the surface resulted from the series of phosphorus and arsenic ion

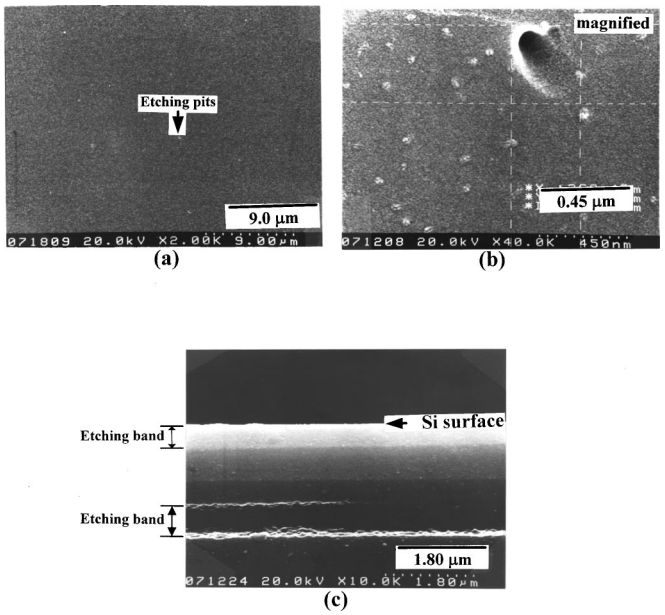

Figure 6. SEM micrographs showing (a) top view, (b) top view (magnified), and (c) cross-sectional view of sample 4 etched in preferential etchant for 30 s.

implantations (P/800 keV, P/220 keV, P/100 keV, and As/50 keV) while the band located at 1.9 to 2.6 μm from the surface is associated with the 1500 keV boron ion implantation.

The fact that extended defects were not found to appear on sample 3 is consistent with the criterion of the extended defect formation because the displaced Si atoms generated by the P^+ and As^+ ions implantations for the construction of a retrograde n-well (sample 3) are well below the critical number that would result in extended defect formation. It has been reported that the critical numbers of displaced Si atoms induced by phosphorus (P^+) and arsenic (As^+) ion implantation that would result in extended defect formation are 5×10^{16} and 1.8×10^{17} cm^{-2}, respectively.[22] There are extended defects and a less clear band of striation in sample 4 extending from the etched substrate surface. Similar to the case of sample 3, P^+ and As^+ ion implantations would not induce the formation of extended defects in sample 4. However, sample 4 also received the high-energy boron ion implantation at 1500 keV to a dose of 3×10^{13} cm^{-2}, which contributed to the formation of the extended defects and the appearance of etching pits near the substrate surface. In addition, we presume that the formation of the lesser clear band of striation at the surface layer was induced by the superposition of the displaced Si atoms resulting from the entire series of high and low energies ion implantations.

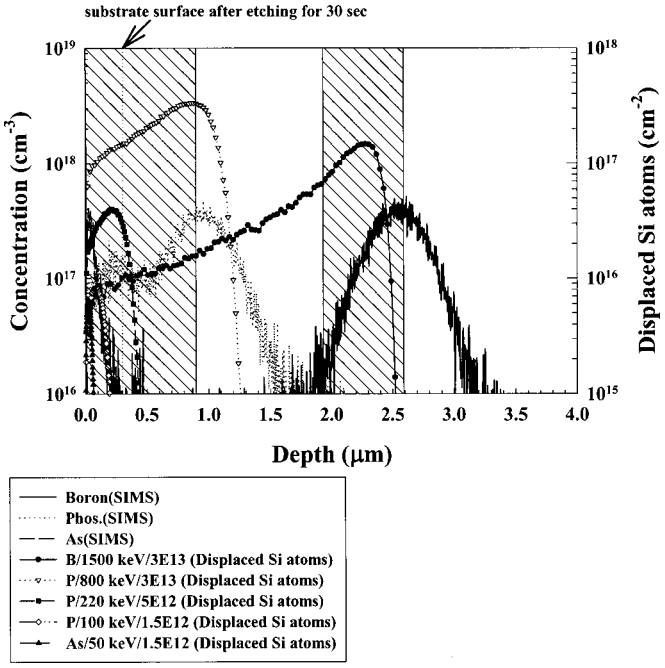

Figure 7. SIMS depth profiles of boron (B), phosphorus (P), and arsenic (As) concentration after thermal annealing at 950°C for 30 min in N_2 ambient and depth profile of displaced Si atoms obtained from TRIM simulation for sample 4.

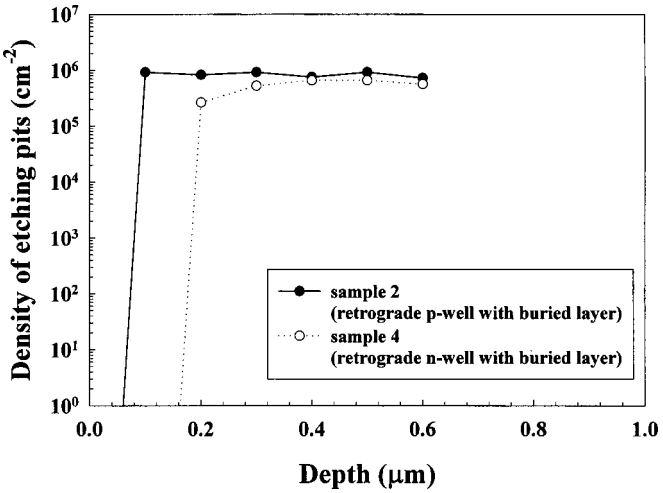

Figure 8. Etching pits distribution for samples 2 and 4.

Figure 8 shows the etching pit distribution for sample 2 (retrograde p-well with buried layer) and sample 4 (retrograde n-well with buried layer). Etching pits of comparable density were found for the retrograde p-well and n-well with buried layer, whereas the extended defects in the retrograde p-well extend closer to the Si surface than those in the retrograde n-well. Similar observations were reported regarding the megaelectronvolts boron ion implantation induced dislocation, studied using TEM and etch pit density counts by Schimmel etching.[20,23,24] The Schimmel etching has a much faster etching rate of 1.5 μm/min, as compared to the etching recipe used in this study (0.6 μm/min). The etching depth can be more easily controlled using the slow etching rate recipe. In this study, etching pits with a density of about 10^6 cm^{-2} were found after removal of a 0.1 μm thick surface layer from the Si substrate (sample 2), whereas the reported data in the literature show that etching pits of comparable density were found after removal of about a 0.6-0.8 μm thick Si surface layer.

Conclusions

This work investigates the implantation-induced extended defects for the retrograde p- and n-well with/without a buried layer after postimplantation thermal annealing at 950°C in N_2 ambient. A preferential etchant of CrO_3/HF mixed solution was used to delineate the defects. It is found that the high-energy ion implantation induced dislocations at the end of the projected range elongated to the top surface of the retrograde well with a buried layer, which was constructed by high-energy boron ion implantation at 1500 keV to a dose of 3×10^{13} cm^{-2}, resulting in etch pits of extended defects at a density of about 10^5 cm^{-2}. The extended defects may have adverse effects on the integrity of gate oxide and p-n junction of devices.

National Chiao Tung University assisted in meeting the publication costs of this article.

References

1. R. D. Rung, C. J. Dell'oca, and L. G. Walker, *IEEE Trans. Electron Devices*, **ED-28**, 1115 (1981).
2. Y. Taur, G. J. Hu, R. H. Dennard, L. M. Terman, C. Y. Ting, and K. E. Petrillo, *IEEE J. Solid-State Circuits*, **20**, 123 (1985).
3. R. A. Martin and J. Y.-T. Chen, *IEEE J. Solid-State Circuits*, **21**, 286 (1985).
4. S. Odanaka, T. Yabu, N. Shimizu, H. Umimoto, and T. Ohzone, *IEEE Electron Device Lett.*, **EDL-10**, 280 (1989).
5. K. Ohyu, T. Suzuki, T. Yamanaka, and N. Natsuaki, *Nucl. Instrum. Methods Phys. Res. B*, **37/38**, 749 (1989).
6. Y. Okazaki, T. Kobayashi, M. Miyake, K. Sakuma, Y. Kawai, M. Tahashi, and K. Kanisawa, *IEEE Electron Device Lett.*, **EDL-11**, 134 (1990).
7. T. Kishimoto, Y. K. Park, M. Takai, Y. Ohno, K. Sonoda, H. Sayama, T. Nishimura, A. Kinomura, Y. Horino, and K. Fujii, *Jpn. J. Appl. Phys., Part 1*, **34**, 6899 (1995).
8. K. Tsukamoto, S. Komori, T. Kuroi, and Y. Akasaka, *Nucl. Instrum. Methods Phys. Res. B*, **59/60**, 584 (1991).
9. K. Tsukamoto, T. Kuroi, S. Komori, and Y. Akasaka, *Solid State Technol.*, **35**, 49 (1992).
10. J. O. Borland and R. Koelsch, *Solid State Technol.*, **36**, 28 (1993).
11. Y. Akasaka, *Nucl. Instrum. Methods Phys. Res. B*, **37/38**, 9 (1989).
12. T. Kishimoto, M. Takai, Y. Ohno, T. Nishimura, M. Inuishi, A. Kinomura, Y. Horino, and K. Fujii, *Nucl. Instrum. Methods Phys. Res. B*, **130**, 524 (1997).
13. W. Morris, L. Rubin, and D. Wristers, in *Proceedings of 1997 International Conference on Ion Implantation Technology*, p. 796 (1997).
14. J.-K. Kim, S.-H. Park, Y.-J. Lee, and Y.-K. Sung, *in Proceedings of the 1997 IEEE International Reliability Physics Symposium*, p. 346 (1997).
15. Y.-T. Jang, T.-H. Huh, and J.-S. Ro, in *Proceedings of 1998 International Conference on Ion Implantation Technology*, p. 959 (1998).
16. M. Tamura, N. Natsuaki, Y. Wada, and E. Mitani, *J. Appl. Phys.*, **59**, 3417 (1986).
17. M. Tamura, N. Natsuaki, Y. Wada, and E. Mitani, *Nucl. Instrum. Methods Phys. Res. B*, **21**, 438 (1987).
18. N. W. Cheung, C. L. Liang, B. K. Liew, R. H. Mutikainen, and H. Wong, *Nucl. Instrum. Methods Phys. Res. B*, **37/38**, 941 (1989).
19. M. Tamura and N. Natsuaki, *Nucl. Instrum. Methods Phys. Res. B*, **39**, 318 (1989).
20. J. Y. Cheng, D. J. Eaglesham, D. C. Jacobson, P. A. Stolk, J. L. Benton, and J. M. Poate, *J. Appl. Phys.*, **80**, 2105 (1996).
21. W. C. Hsu, M. C. Chen, and M. S. Liang, *J. Electrochem. Soc.*, **147**, 3111 (2000).
22. R. J. Schreutelkamp, J. S. Custer, J. R. Liefting, W. X. Lu, and F. W. Saris, *Mater. Sci. Rep.*, **6**, 275 (1991).
23. K. K. Bourdelle, D. J. Eaglesham, D. C. Jacobson, and J. M. Poate, *J. Appl. Phys.*, **86**, 1221 (1999).
24. K. S. Jones, C. Jasper, and A. Hoover, *Appl. Phys. Lett.*, **78**, 1664 (2001).